A full wavefield approach to marine survey planning

Chloé Lazizi[1]*, Stefan Jetschny[1], Morten W. Pedersen[1] and Alba Ordoñez[1] present a full wavefield approach to survey design, providing an insight into optimal acquisition parameters taking account of the application of separated wavefield imaging.

Introduction

Conventional processing of 3D marine seismic data based on primary reflections can suffer from strong acquisition related footprint. The problem manifests as gaps in the data because the water bottom and shallow features lack full illumination in shallow water data. The phenomenon is most obvious at the water bottom and gradually heals with increasing depth. This degradation of the shallow image is particularly problematic for surveys that target geohazard evaluation. Furthermore, accurate and continuous water bottom information can be crucial for multiple removal techniques that are required for successful imaging of deeper targets (Brittan et al., 2011).

Separated wavefield imaging is a technique that has been developed to image the subsurface using any order of sea-surface multiples (Whitmore et al., 2010). The method requires the separation of upgoing and downgoing wavefields using multi-sensor marine streamer recordings (Carlson et al., 2007). By considering sea-surface reflections, receivers act as virtual sources, which provide increased lateral illumination and angular diversity compared to primary only reflections (Figure 1). Lu et al. (2013) demonstrated that imaging with sea-surface multiples is a valuable tool, providing a continuous water bottom image by reducing the acquisition related footprint and gives improved resolution of shallow structures. Separated wavefield imaging can therefore be used to obtain high-quality images from data acquired using operationally efficient acquisition configurations.

Geophysical survey planning evaluates the image quality that can be obtained using different acquisitions configurations to determine the most effective solution for a particular target. Current procedures focus on primary reflections and ensure fast turnaround time by using ray tracing and plane layer modelling (e.g. Day and Rekdal, 2005). By focusing solely on primary reflections, these methods ignore the contribution of sea-surface reflections and can give a misleading impression of the image quality that can be obtained by using a particular acquisition configuration. Lu et al. (2015) defines a list of acquisition factors that control the effectiveness of separated wavefield imaging which need to be addressed in a survey planning phase.

In this paper, we present a methodology that enables the complexity of the separated wavefield imaging to be included in the survey planning phase. The method uses finite difference modelling and a one-way wave-equation migration while maintaining the fast turnaround necessary for survey planning. The

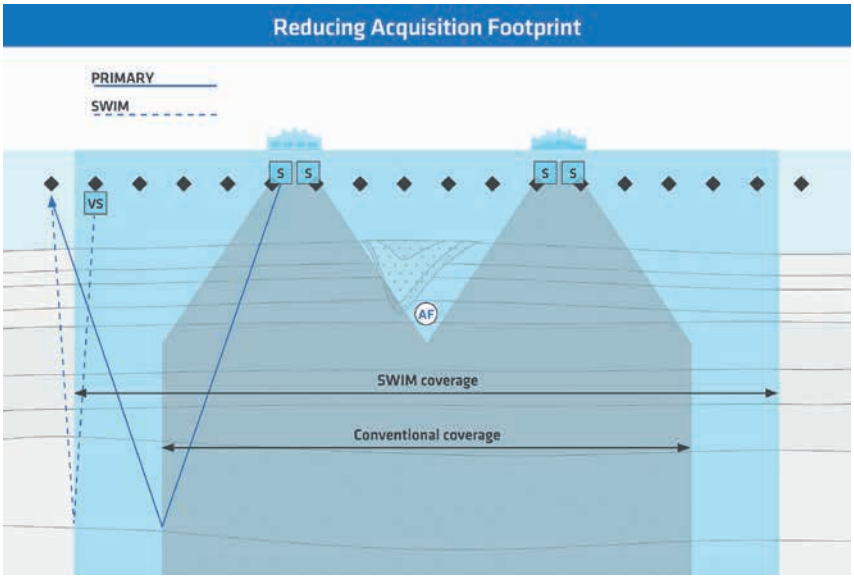

Figure 1 Turning the receiver spread into virtual sources (VS) increases lateral illumination and angular diversity. Using separated wavefield imaging in shallow water fills in gaps in near-surface coverage, reducing the acquisition footprint (AF).

[1] PGS
* Corresponding author, E-mail: chloe.lazizi@pgs.com

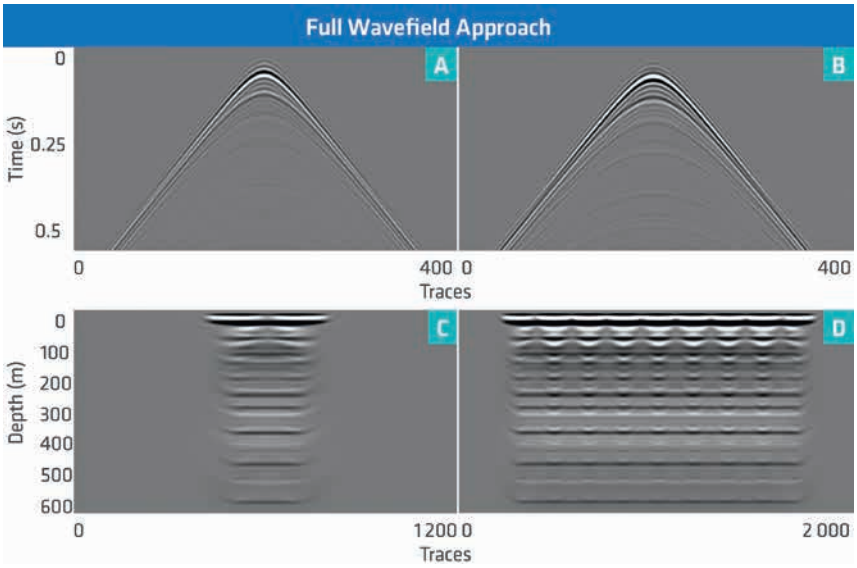

Figure 2 Upgoing and downgoing wavefields (a and b respectively) are obtained from wavefield separation of modelled pressure and vertical particle velocity data. These wavefields are the input to the one-way wave-equation migration (c, crossline view). The migrated shot is duplicated to mimic a more realistic acquisition with several shots and sail lines (d, crossline view of eight sail lines).

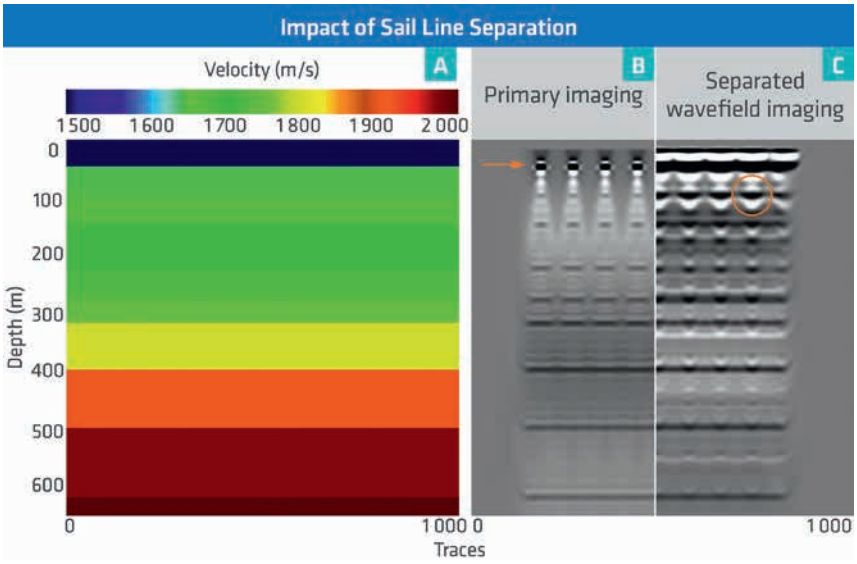

Figure 3 a) 2D compressional velocity model used for separated wavefield and primary imaging. This model is an approximation of the shallow part of a survey acquired offshore Ivory Coast. b) Synthetic primary image. c) Synthetic separated wavefield image. The arrow shows the water bottom depth where the migration response is picked. The red circle shows the overlapping zone between two adjacent sail lines.

principles behind this full wavefield approach will be described and results are presented.

Methodology

The full wavefield approach to survey design involves modelling of primary and multiple reflections followed by separated wavefield imaging. As in traditional survey planning, we base our studies on plane layer models. However, we have chosen to perform the modelling using a finite difference approach (e.g. Mittet et al., 1988) as this method models all multiples from all interfaces. A representative model can be built using existing knowledge of the target area. Different acquisition configurations are parameterized by defining the number of cables, cable and sail line separations, and receiver and source depths.

In this paper, we have emulated a single source acquisition using a point source which includes frequencies up to 80 Hz. Alternative source configurations (e.g. dual and triple source) and more realistic representations of sources used in the field that incorporate directivity can easily be included for more detailed analysis. However, we have found that a number of useful insights can be obtained from the single source experiment. In the case of a horizontally layered model, it is sufficient to model a single shot. This approximation permits the use of relatively expensive finite difference modelling for survey planning studies that require a rapid turnaround.

The finite difference modelling is run using only acoustic propagation and an active sea-surface. Two wavefields are generated: the total pressure wavefield and the total vertical particle velocity wavefield. These wavefields contain primary and multiple reflections, refractions and their multiples, the receiver side ghost of all these arrivals and the direct wave. The direct wave and refracted energy are removed by muting both wavefields. This is done prior to the wavefield separation, to compute the upgoing and downgoing wavefields (Figure 2a and 2b) using the method described by Carlson et al. (2007).

A one-way wave-equation migration is run using the upgoing and downgoing wavefields. In this case, both wavefields are downward extrapolated to the depth of the reflectors. The two extrapolated wavefields are then imaged using a deconvolution imaging conditions as described by Whitmore et al., (2010). The

result of the one-way wave-equation migration is the migrated image derived from a single shot (Figure 2c). The final step is to duplicate this migrated image to mimic a more realistic acquisition with several shots and sail lines (e.g. Figure 2d has eight sail lines). In this manner, a representative migrated image can be obtained for any acquisition configuration.

Acquisition related footprint

Wide sail line separations are one of the main causes of strong acquisition footprints. However, reducing the sail line separation increases the time and cost of the acquisition. By using the sea-surface reflections, imaging with separated wavefields decreases the impact of the sail line separation and improves shallow imaging. This imaging technique can allow cost effective acquisition configurations utilizing wide sail line separation to be deployed without loss of image quality. The aim of the first survey planning application is to reproduce the impact of the sail line separation in a synthetic model and estimate the depth to which separated wavefield imaging provides an uplift compared to primary imaging.

Sail line separations are typically chosen to be half the width of the streamer spread to ensure continuous subsurface coverage. For the purposes of evaluating the impact of sail line separation on the image, we assume dense receiver sampling. Figure 3a shows a plane layer approximation of shallow geology, which was used to model synthetic data as previously described. We modelled an acquisition configuration comprising 160 cables separated by 6.25 m, providing a spread width of 1000 m. Two images were then computed: one using only primary reflections (Figure 3b) and the other using primary and multiple reflections (Figure 3c). In both cases, the same wave-equation based imaging algorithm was used. For the primary imaging, the receiver wavefield was the upgoing primaries and the source wavefield was modelled internally by a point source. Separated wavefield imaging used the receiver wavefield as the total upgoing wavefield (including multiples) and the source wavefield was the total downgoing wavefield excluding the direct arrival. Eight sail lines spaced 500 m apart were modelled. Strong acquisition related footprint can be observed between the sail lines for primary imaging (Figure 3b) that heal with increasing depth. Similar patterns can be observed in field data. With separated wavefield imaging (Figure 3c), the footprint is reduced and the image provides continuous illumination of the shallow reflectors. The illumination gaps seen in the primary image are filled using information contained in the multiples. Moreover, the image from separated wavefield imaging shows areas where the amplitude is stronger (red circle in Figure 3c). This is caused by the increase of angular diversity and lateral illumination coming from the sea-surface multiples. This area is an overlapping zone originating from the illumination of two adjacent sail lines. These amplitude variations are reduced in post-processing, whereas the amplitude reduction associated with poor illumination at sail line boundaries in the primary image are too severe to be recovered. The high amplitude overlapping zones in the separated wavefield image occur in the same location as the gaps in the primary image. This illustrates how separated wavefield imaging provides continuous illumination of the water bottom and shallow targets.

To estimate the depth at which primary imaging gives equivalent acquisition illumination to separated wavefield imaging, the amplitude of the migration response of each reflector was extracted. In Figure 4a, examples of the migration response from primary imaging and separated wavefield imaging are shown. The migration response from primary imaging and separated wavefield imaging present a peak-to-trough ratio of approximately 35 dB and 4 dB respectively. By calculating the ratio between the maximum and minimum amplitude, the imprint of the footprint effect can be quantified for each reflector. The amplitude of the footprint is shown as a function of the depth for all reflectors in Figure 4b. The primary image shows a large sail line related footprint at the water bottom that reduces with increasing depth. For the separated wavefield image, the variations are small and are invariant with depth. For this example, the sail line related footprint of primary imaging and separated wavefield imaging intersect at a depth of 350 m. At a depth shallower than 350 m, separated wavefield imaging fills the gaps present in the primary image. Below this depth, any additional information provided by separated wavefield imaging is less significant. This is consistent with numerous field examples from West Africa.

This example demonstrates that sail line-related footprint can be quantified during survey planning and the depth to which

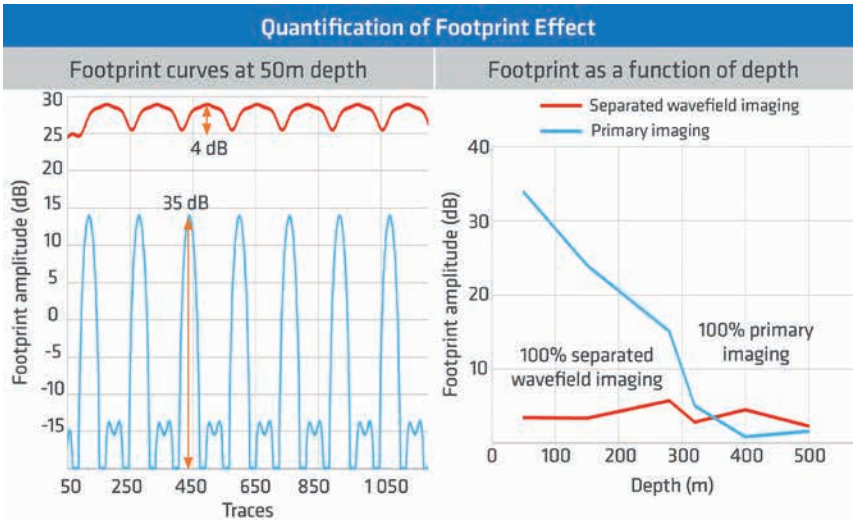

Figure 4 a) Footprint curves for separated wavefield imaging (red) and primary imaging (blue) at the water bottom depth (50 m). b) Footprint as a function of depth for primary imaging (blue) and separated wavefield imaging (red).

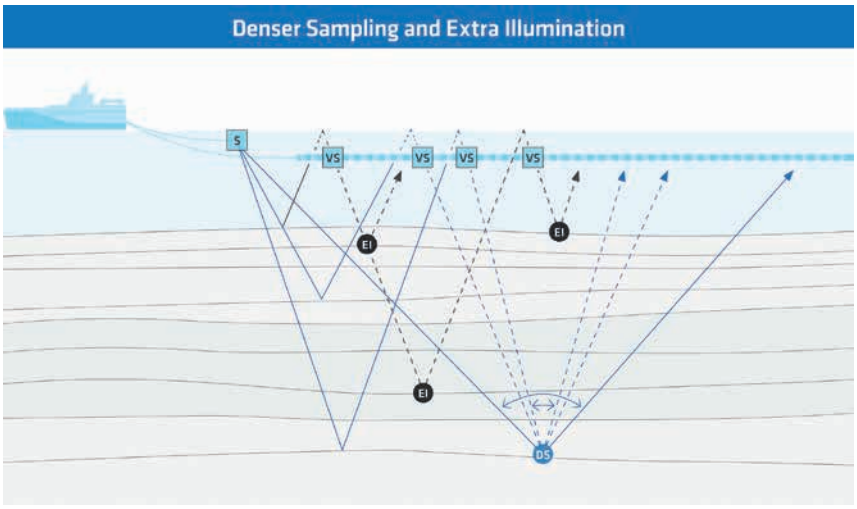

Figure 5 Separated wavefield imaging uses receivers as virtual sources (VS) and delivers extra illumination (EI) and denser sampling (DS). Primary reflections (straight blue lines) have wider angles while multiple reflections have smaller angles (dashed blue lines).

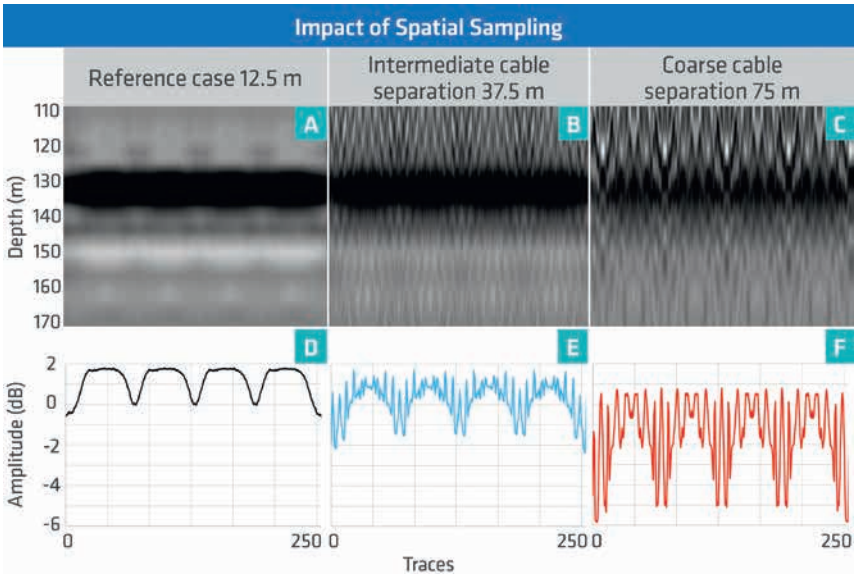

Figure 6 Water bottom images (a, b and c) and corresponding footprint curves (d, e and f) of synthetic data simulating three different cable separations using separated wavefield imaging modelling.

separated wavefield imaging provides an uplift over the primary imaging can be predicted. The results depend, among other things, on water depth, seabed reflectivity, cable spread width and sail line separation. This information can be used to inform on a processing strategy that arises from a particular choice of acquisition configuration.

Wavefield sampling requirements

In the previous application, sufficient sampling in the crossline was assumed and, the effects of cable separation were not considered. However, crossline sampling and the associated aliasing effects are important considerations for all imaging approaches. Primary reflections have wider reflection angles compared to multiple reflections (Figure 5). Consequently, the primary wavefield might be more aliased than the multiple wavefield.

On this basis, it is expected that separated wavefield imaging will be less susceptible to image distortion due to coarse sampling. However, for primary imaging only the upgoing wavefield is subject to aliasing: the source wavefield, which is an impulse wavelet, is modelled, and is not affected by the cable separation. For separated wavefield imaging, both upgoing and downgoing wavefields are potentially aliased. Therefore, the effect of spatial sampling on separated wavefield imaging is more complex than the primary imaging case and needs to be specifically investigated.

We quantify the impact of spatial sampling, by comparing the images obtained for different cable separations with an over-sampled reference case. As an example, we chose a model with a water bottom at 130 m depth and a velocity contrast typical of the North Sea. Separated wavefield imaging was performed and the results are presented in Figure 6.

The reference case is shown in Figure 6a. The images for two other cases with wider cable separations (37.5 and 75 m) are displayed in Figure 6b and 6c. The upper raw images in Figure 6 represent the water bottom, which is the target horizon for this study. The water bottom is the reflector that suffers most degradation due to coarse sampling, and these effects will decrease with depth as the reflection angles at the target horizons become closer to zero. The coarser the cable separation is, the stronger the effects on the illumination of the water bottom. To quantify the influence of the cable separation, the amplitudes were picked along the water bottom reflector (Figure 6d, 6e and 6f). The migration responses exhibit the same background

amplitude trend as the reference case, with trace-to-trace fluctuations superimposed. The coarser the cable separation is, the more variation is observed.

To isolate the effect of the spatial sampling, the footprint curve for the reference case was subtracted from those for the wider cable separations. These differences are displayed in Figure 7. Root mean square values of the difference are displayed as dashed lines. These values represent an average value of the image distortion caused by coarse spatial sampling. A user threshold (black curve in Figure 7) can be applied to define acceptance levels in the image. This threshold is specified for either acquisition or imaging purposes. Given that it is not efficient nor practical to acquire data with a cable separation of 12.5 m, this approach helps to determine the wavefield sampling required to reduce the image distortion to an acceptable level. In this example, for the chosen threshold of 0.8 dB, a crossline sampling of 37.5 m is required to obtain a good image. This can be obtained by a 2:1 resampling from a typical acquisition cable separation of 75 m. If a coarser cable separation is used in acquisition, or the permitted threshold is reduced, the degree of resampling that is required will be increased. This modelling method allows these trade-offs between acquisition efficiency and image quality to be evaluated quantitatively. Note that the water bottom reflector represents the extreme case. Similar analysis could be applied to deeper target horizons if needed, and would result in less stringent wavefield sampling requirements.

The method was calibrated using a field data example from the North Sea acquired with a cable separation of 75 m. The North Sea synthetic data was performed using a similar model to those in Figure 6 and 7, but with a degree of roughness introduced at the seafloor. Cable feathering was observed during the acquisition, hence it was also included in the modelling. These changes were introduced to make the synthetic modelling more representative of the field acquisition. Water bottom images from the acquired and synthetic data are displayed in Figure 8a and Figure 8b respectively. Visual comparisons of these images show that the effect of the cable separation is similar in both images. To make a quantitative comparison, the migration response was picked along the seafloor reflector for both cases (Figure 8c). The two curves exhibit similar characteristics. Feathering and seafloor roughness complicate the overlap between two adjacent sail lines, the result being less symmetrical than Figure 6 for horizontal reflectors and no feathering. Furthermore, the degree of variation arising from coarse spatial sampling is reduced. This example

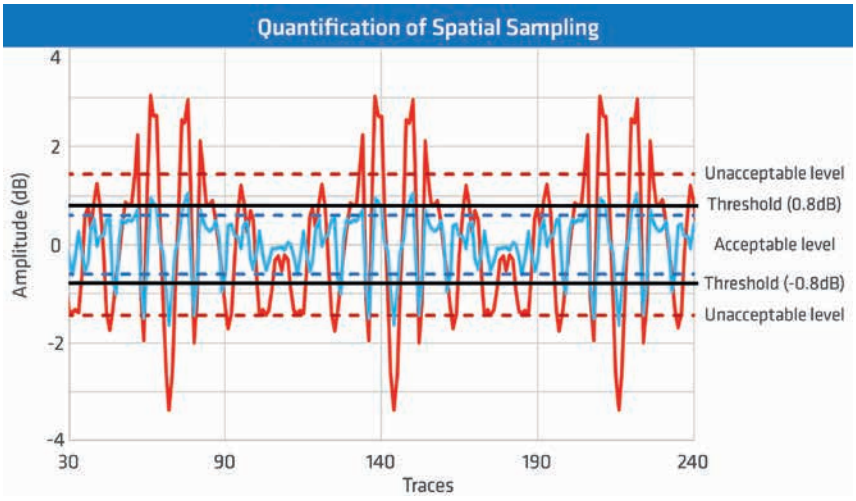

Figure 7 Footprint for the intermediate (blue) and coarse cable separation cases, 37.5 and 75 m respectively. The black line represents a suggested acceptance threshold.

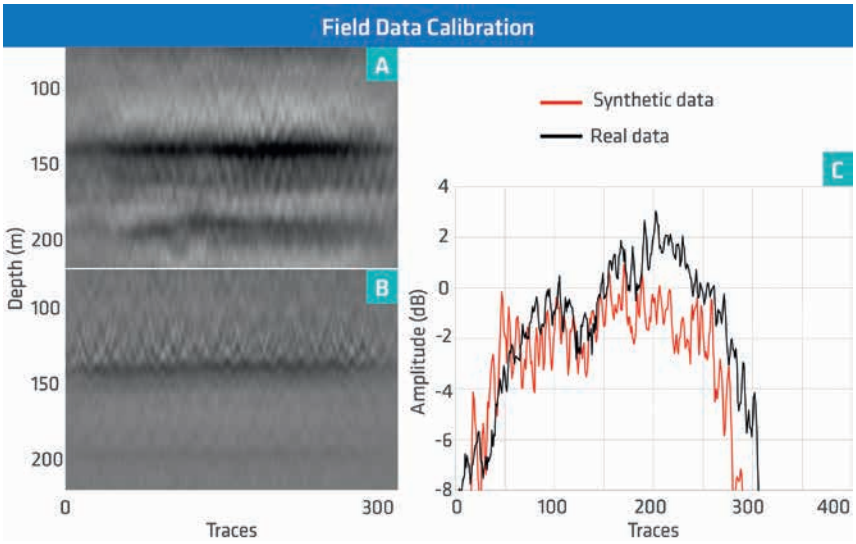

Figure 8 Water bottom images of the field data (a) and the synthetic data (b) for a cable separation of 75 m. c) Footprint curves picked at the water bottom for the field data (black) and for synthetic data (red).

demonstrates that the effect of cable separation in field data can be predicted using synthetic modelling by including feathering and realistic sea bottom characteristics. The prediction obtained from a horizontal seafloor reflector and straight cables represents a worst case scenario but provides a reasonable estimate of the required wavefield sampling.

Resolution based on wavefield sampling

As demonstrated in the previous application, the spatial sampling of the wavefield obtained from typical marine acquisition configurations often needs to be refined prior to migration. The accuracy of the resampled wavefield depends on the receiver spacing in acquisition as well as the subsurface complexity. In this third application of the full wavefield approach to survey modelling, the cable separation is again the focus as it is a key component for wavefield reconstruction.

In this case, a 2.5D model was built, allowing more complexity in the shallow section. Nine faults with various throws (10, 25 and 50 m) and widths (50, 100 and 200 m) were added, resulting in a more complex modelled wavefield (Figure 9). It

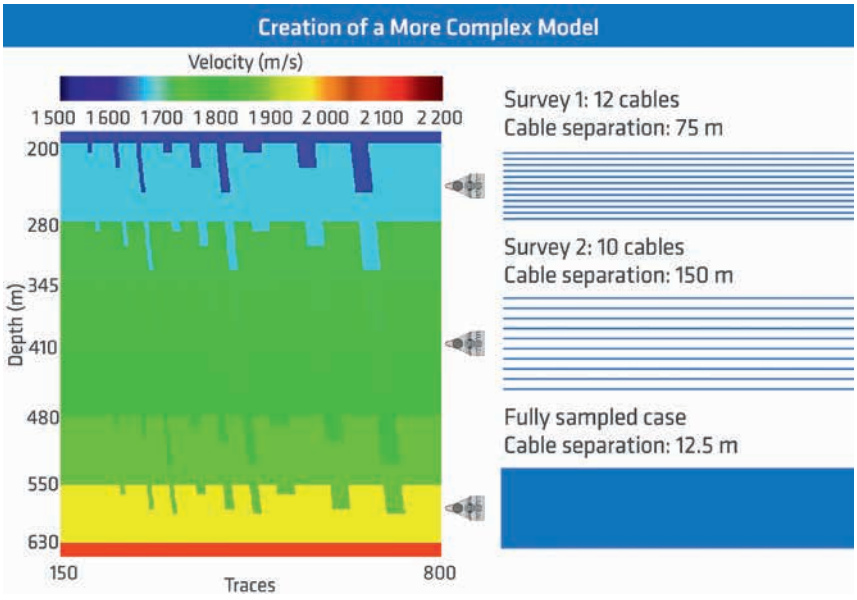

Figure 9 2.5D models faulted plane layer compressional velocity model (left) used for the separated wavefield imaging resolution study. A crossline plane is shown perpendicular to the sail line direction. The two survey configurations (right) used for the study with different cable separations, reconstructed to 12.5 m and the fully sampled reference case modelled with a cable separation of 12.5 m.

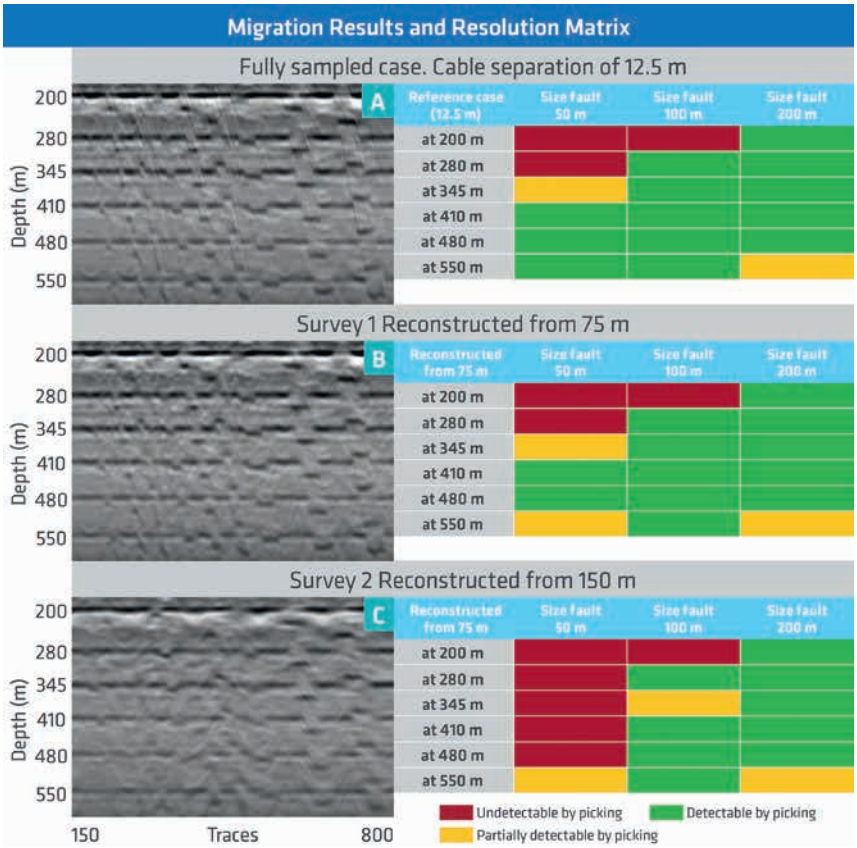

Figure 10 Panel of migration results as a result of separated wavefield imaging resolution study with respect to three different initial cable separations where two are reconstructed to 12.5 m surface sampling. The corresponding resolution matrix shows a qualitative interpretation of picking along horizons at selected target depths.

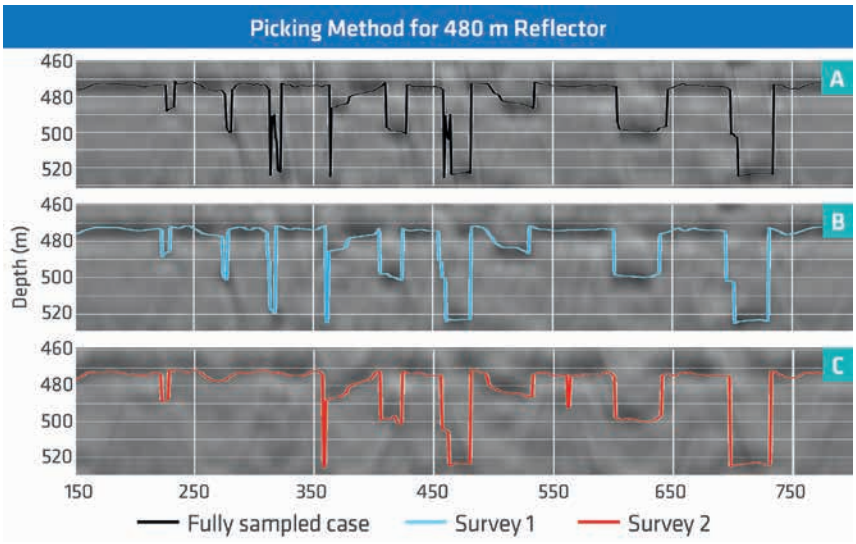

Figure 11 Picking method for the reflector at 480 m depth in the model: a) picking curves of the fully sampled survey (cable separation of 12.5 m), b) picking curve for survey 1 (12 cables spaced by 75 m), c) picking curve for survey 2 (10 cables spaced by 150 m). The corresponding migrated images are displayed in the background.

is therefore possible to observe the impact of the reconstructed wavefield on resolution. We can model one or more surveys with realistic cable separations, and compare the images obtained after wavefield reconstruction with a reference case. In this example, the two test surveys have a cable separation of 150 m and 75 m. The wavefields obtained from these two acquisition configurations are undersampled, and wavefield reconstruction to 12.5 m sampling was performed prior to imaging. The resulting images were compared to the reference case obtained from data modelled with a cable separation of 12.5 m. The faulted model and different acquisition configurations are displayed in Figure 9. To image the faults, several shots were modelled to cover the full extent of the faulted area.

Spatial resampling based on an anti-alias anti-leakage Fourier-based interpolation algorithm was performed prior to migration (Schonewille et al., 2009). Depending on the wavefield sampling in the input data, the resolution of the depth image varies making it possible to identify the presence of faults in the input velocity model. As expected, the reference geometry with fully sampled receiver spreads shows very good image resolution (Figure 10a). When resampling from a typical cable separation of 75 m to the reference cable separation, the resolution is essentially the same as the fully sampled case (i.e. all the faults appear to be imaged properly – Figure 10b). However, when resampling from a coarser cable separation of 150 m, the image resolution decreases (Figure 10c).

To quantify the resolution, a simple picking algorithm was applied along the target reflectors to objectively determine if the faults have been imaged. The picking algorithm indicates how accurately the fault has been imaged (width and throw of each fault as a function of depth). An example is presented in Figure 11. For the fully sampled case (Figure 11a) and for the reconstructed case from 75 m cable separation (Figure 11b), the picking is able to detect all the faults while for the reconstructed case from 150 m cable separation (Figure11c), the picking is not able to detect the smallest faults. Results are then colour-coded and displayed in a resolution matrix (bottom of Figure 10) to simplify the visualization of the image resolution that has been achieved. The fully sampled case shows very good resolution with all the faults imaged apart from very small features in the shallow part. The resampled case from 75 m cable separation exhibits a similar resolution matrix to the fully sampled case. However, for the 150 m cable separation case, the smallest faults are not as easily detectable at all the depths.

Based on the plane layer properties and the candidate survey configuration, resolution of imaging with separated wavefield can now be tested objectively and the optimal wavefield sampling (e.g cable separation) that satisfies the imaging requirements for this particular case can be decided. Note that the results depend on the seafloor depth, the geology and the structural complexity of the area.

Conclusion

Separated wavefield imaging is a technique that resolves the acquisition related illumination footprint observed in conventional seismic imaging in shallow water data. However, to benefit fully from the method, the acquisition parameters need to be planned accordingly. Survey planning methods are typically based on ray tracing and consider only primary imaging for reasons of efficiency. Using 1D and 2.5D models, the modelling and migration cost can be reduced, and a full wavefield approach can be applied in survey planning, thereby providing a means to assess challenges specifically related to imaging sea-surface reflections.

The full wavefield approach provides a solution to identify and address any potential separated wavefield imaging challenges during the survey planning phase. The depth to which separated wavefield imaging provides an uplift compared to primary imaging can be determined. Once this information is known, the optimal wavefield sampling required to limit image distortion can be estimated. For practical and efficiency reasons, this optimal wavefield sampling is often too fine to be acquired in the field. However, wavefield resampling prior to migration can be performed and its influence on the final image can be quantified. Based on the survey configuration and the geology, the optimal cable separation that satisfies the imaging requirements after wavefield resampling can now be objectively tested.

This new suite of tools enables the cost-benefit trade-off between efficient acquisition and image quality to be assessed during survey planning, and takes into account advanced imaging techniques such as separated wavefield imaging.

Acknowledgements

We would like to thank PGS for permission to publish this paper. We are grateful for all fruitful discussion with our colleagues Marina Lesnes, Anthony Day, Tony Martin and Manuel Beitz that have contributed to this work.

References

Brittan, J., Martin, T., Bekara, M. and Koch, K. [2011]. 3D shallow water demultiple – extending the concept. *First Break*, **29**(7), 97-101.

Carlson, D., Long, A., Söllner, W., Tabti, H., Tenghamn, R. and Lunde, N. [2007]. Increased resolution and penetration from a towed dual-sensor streamer. *First Break*, **25**(12), 71-77.

Day, A. and Rekdal, T. [2005]. Determining infill specifications based on geophysical criteria. *85th SEG Technical Program*, Expanded Abstracts, 80-83.

Lu, S., Whitmore, N.D. and Valenciano, A.A. [2013]. Challenges and opportunities in 3D imaging of sea-surface related multiples. *83rd SEG Technical Program*, Expanded Abstracts, 4111-4115.

Lu, S., Whitmore, D., Valenciano, A. and Chemingui, N. [2015]. Separated-wavefield imaging using primary and multiple energy. *The Leading Edge*, **34**(7), 770-778.

Mittet, R., Holberg, O., Arntsen, B. and Amundsen, L. [1988]. Fast Finite-Difference Modeling of 3-D Elastic Wave Propagation. *SEG Technical Program*, Expanded Abstracts, 1308-1311.

Schonewille M., Klaedtke, A., Vigner, A., Brittan, J. and Martin, T. [2009]. Seismic data regularization with the anti-alias leakage Fourier transform. *First break*, **27**(9), 85-92.

Whitmore, N.D., Valenciano, A.A., Söllner, W. and Lu, S. [2010]. Imaging of primaries and multiples using a dual-sensor towed streamer. *80th SEG Technical Program*, Expanded Abstracts, 3187-3192.